

OPEN

Mesoporous bimetallic Fe/Co as highly active heterogeneous Fenton catalyst for the degradation of tetracycline hydrochlorides

Junchao Li, Xuhua Li, Jindong Han, Fansheng Meng, Jinyuan Jiang*, Jiao Li, Chunlian Xu & Yun Li

Mesoporous bimetallic Fe/Co was prepared as a Fenton-like catalyst to degrade the tetracycline hydrochlorides (TC). The nanocasting strategy with KIT-6 as a hard template was carried out to synthesize the mesoporous bimetallic catalyst. The mesoporous bimetallic Fe/Co catalyst was characterized by X-ray diffraction (XRD), transmission electron microscopy (TEM), nitrogen adsorption-desorption isotherms, and Brunauer-Emmett-Teller (BET) method. The results showed that the catalyst has significant nanofeatures; the surface area, pore size, and particle size were $113.8 \text{ m}^2\text{g}^{-1}$, 4 nm, and 10 nm, respectively. In addition, the effects of the operating parameters, such as the iron-to-cobalt ratio, pH, H_2O_2 , and initial TC concentrations on its catalytic performance were investigated. The best operating parameters were as follows: iron-to-cobalt ratio = 2:1 to 1:1, pH = 5–9, H_2O_2 : 30 mmol, initial TC less than 30 mg/L. Furthermore, the mesoporous bimetallic Fe/Co showed a good performance for degrading TC, achieving a removal rate of 86% of TC after 3 h under the reaction conditions of $\text{H}_2\text{O}_2 = 30 \text{ mmol}$, mesoporous bimetallic Fe/Co = 0.6 g/L, TC = 30 mg/L, pH = 7.0, and temperature = 25.5 °C. The mesoporous bimetallic Fe/Co catalyst shows good stability and reusability. This work demonstrated that mesoporous bimetallic Fe/Co has excellent catalytic efficiency, smaller amounts of leached ions, and wider pH range, which enhance its potential applications.

Antibiotics constitute a new class of water contaminants of emerging concern with adverse effects on the ecological environment¹ as larger amounts of antibiotics are frequently detected in surface water² and municipal sewage treatment plants³. Antibiotics are difficult to be treated by microorganisms and physical adsorption; in fact, only 20–30% of antibiotics can be biodegraded by microorganisms⁴ and removed by physical adsorption, resulting in complicated post-treatment problems of sorbents⁵. Advanced oxidation technologies (AOTs), based on the generation of highly reactive hydroxyl ($\bullet\text{OH}$) free radicals, are used in wastewater treatment plants to remove various pollutants. They are simple processes with low energy consumption and without any secondary pollution and thus considered to be promising strategies^{6–8}.

As one of the AOTs, heterogeneous catalysts have displayed satisfactory performance in Fenton-like processes; the pH usage limits are further alleviated without the precipitation of iron hydroxide⁹. Iron minerals possess the advantages of the low band gap (2.2 eV), low cost, and nontoxicity¹⁰. However, decreased degradation rates and large consumption of H_2O_2 limit the practical applications of heterogeneous Fenton-like catalysts^{11,12}. The heterogeneous Fenton catalyst efficiency can be improved by increasing the surface area, enhancing their dispersion, and introducing suitable transition metals into heterogeneous catalysts^{13–16}. Nanocatalysis is one of the many practical applications of nanotechnology^{17–19}. Development of a nanocatalyst with a high surface area can accelerate Fenton-like reactions because the active sites are located on the surface and the catalytic performance of the nanocatalyst depends on the effect of “smaller particle size, higher activity^{20,21}”.

Due to the flexible synthesis method, unique physical properties, easy surface functionalization, and good biocompatibility, mesoporous nanomaterials are increasingly used in adsorption, separation, catalysis, energy storage, and biomedical applications, especially as multi-functional drug delivery carriers for loading various chemical drugs, biomacromolecules, genes, and as a multifunctional diagnostic platform for composite magnetic

State Key Laboratory of Environmental Criteria and Risk Assessment, Chinese Research Academy of Environmental Sciences, Beijing, 100012, China. *email: jiangjy@craes.org.cn

properties^{22–25}. In addition, the heterogeneous catalysts with transition metals improve not only the catalytic performance but also the reaction conditions under the synergistic effect of multimetals^{16,20,21,26}.

This study aims to use KIT-6 as a template to prepare highly ordered mesoporous iron-cobalt heterogeneous catalysts¹². The strategy of nanocasting (by solid phase method) accelerates the Fenton-like reaction and improves reaction conditions. Additionally, a new mechanism was proposed based on the experimental data analysis and literature review. Finally, the stability and reusability of the catalyst were evaluated.

Methods

Reagents. Ferric nitrate ($\text{Fe}(\text{NO}_3)_3 \cdot 9\text{H}_2\text{O}$), cobalt nitrate ($\text{Co}(\text{NO}_3)_2 \cdot 6\text{H}_2\text{O}$), butyl alcohol, hydrochloric acid (HCl), sodium hydroxide (NaOH), tetraethylorthosilicate (TEOS), and ethanol for preparation of ordered meso-Fe/Co were purchased from Sinopharm Chemical Reagent Co., Ltd., SCRC, China. H_2O_2 (30% v/v), ethanol, isopropanol, and tetracycline (TC) hydrochloride were purchased from Aladdin and triblock copolymer Pluronic P123 ($M_w = 5800$, EO20PO70EO20) from Sigma–Aldrich. The purity of the agents used was no lower than analytical grade, and no further purification work was performed on the agents. Deionized water was used for all experiments.

Preparation of meso-Fe/Co. Meso-Fe/Co catalyst was prepared by template synthesis, and template material KIT-6 was synthesized by classical method^{27,28}. $\text{Co}(\text{NO}_3)_2 \cdot 6\text{H}_2\text{O}$, $\text{Fe}(\text{NO}_3)_3 \cdot 9\text{H}_2\text{O}$ and KIT-6 powder are evenly mixed, and ground using an and appropriate amount of ethanol is added to dissolve iron salt and cobalt salt. The mixture was soaked in ethanol solution for 12 hours to fully immerse the ethanol salt solution into KIT-6. The mixed solution was transferred to the water bath pot for evaporation, the obtained solid sample was further transferred to the tube furnace for calcining at 600 °C for 5 hours. The sample was cooled to room temperature and transferred to 2M NaOH solution for 24 hours under the condition of stirring, and then was further filtered, washed and dried. Finally, the reduction was conducted in a 450 °C muff furnace for 2 hours with the heating rate of 5 °C min⁻¹ in hydrogen atmosphere.

Experimental procedure. Catalytic performance of mesoporous Fe/Co was tested at room temperature by using a constant temperature shaker (200 r/min) and a flask (1000 mL). The reaction system consists of catalyst (0.6 g/L), target contaminant (TC = 30.0 mg/L, volume = 200 mL, pH7.0 ± 0.5) and oxidant (H_2O_2 , 3.0 mL). The reaction time was set at 180 minutes, and the pH value was adjusted by using HCl (0.5 M) and NaOH (0.5 M). Three parallel experiments were carried out for this study. The prepared catalysts were collected and stored in nitrogen environment, and their structures were characterized by SEM, TEM, XRD and BET. The reusability of the catalyst was evaluated by collecting the catalyst with magnet and reusing the catalyst for the next reaction under similar experimental conditions.

Sample analysis. Concentration analysis test of tetracycline hydrochloride (TC) during catalytic reaction: Samples with different reaction times were filtered by 0.45 μm nylon membrane and tetracycline hydrochloride (TC) concentrations were analyzed by Jena uv-vis-vis spectrometer (SPECORD200PLUS) at 356 nm. Spectrophotometry was used to analyze the concentration of Fe and Co in the color developing solution at 510 nm by the absorbance of the color developing solution using 1, 10-phenanthroline^{29,30} and 5-cl-padab³¹, respectively. The total organic carbon was determined by a Multi 3100 TOC/TN analyzer (Analytik Jena AG). For the TOC analysis test, all samples were immediately treated with scavenging agents (0.05 M Na_2SO_3 , 0.05 M KH_2PO_4 , 0.05 M KI and 0.02 M NaOH) to obtain accurate TOC values^{14,32}.

The sample structure was qualitatively analyzed by field emission scanning electron microscope FE-SEM; Hitachi S-4700 II at 15.0 kV accelerated voltage, JEOL JEM 2010 F electron microscope at 200 kV and physical D/max-2400X-ray diffractometer with Ni filter Cu K⁺ radiation, respectively. Micromeritics ASAP 2020 was used to analyze the sample surface area and pore diameter distribution by N₂ adsorption and desorption, and the sample surface area was calculated by Brunauer_Emmett_Teller (BET) method.

Results and Discussion

Morphology and structure. The characterization of catalysts helps to a better understanding of the relationship between catalytic properties of catalysts and their physical structures. SEM and TEM images clearly show perfect micropores and physical structure, uniform shape and smooth surface. In order to further study the mesoporous structure of the catalyst, the sample was described. According to the analysis of the sample SEM image (Fig. 1) and TEM image (Figs 2, 3), the catalyst effectively entered the intermediate pore structure of the template during the preparation process. According to the statistical analysis, the catalyst sample is composed of spherical particles of different sizes, and the catalysts between particles are mainly distributed in the range of 2 to 10 nm. The aperture of the KIT-6 was about 6.8 nm (Fig. 4), which was consistent with the results of previous studies¹².

XRD analysis of Mes-Fe/Co shows that phase analysis of catalyst according to PDF card 22-0864#, 22-1086#. In $2\theta = 35.1^\circ$ and 41.4° and 50.4° and 62.9° and 67.3° and 74.2° and 88.6° there is obvious diffraction peak, corresponding alloy (220) (311) (222) (400) (422) (511) (440) and (533) plane³³ (Fig. 5), showed that the method is used to Fe/Co bimetallic catalyst was successfully achieved. The position and relative strength of the diffraction peak of the synthetic bimetallic Fe/Co catalyst are consistent with the standard XRD data of the spinel (No. 22-1086 and No. 03-0864).

The results of N₂ adsorption-desorption isotherm study on the specific surface area and porosity of samples show that the adsorption isotherm curve of the sample is H3 hysteresis loop IV (Fig. 4), which is a typical mesoporous characteristic structure with a specific surface area of 135.8 m² g⁻¹, much higher than that of commercial Fe₃O₄ (~2 m² g⁻¹)³⁴. The results of pore diameter of catalyst by Barrett-Joyner-Halenda (BJH) method showed that the pore diameter of the catalyst is mainly in the range of 1–40 nm, about 40% pore is distributed in the range of 2–10 nm mesoporous³⁵, and about 20% pore size is distributed in the range of 10–20 nm.

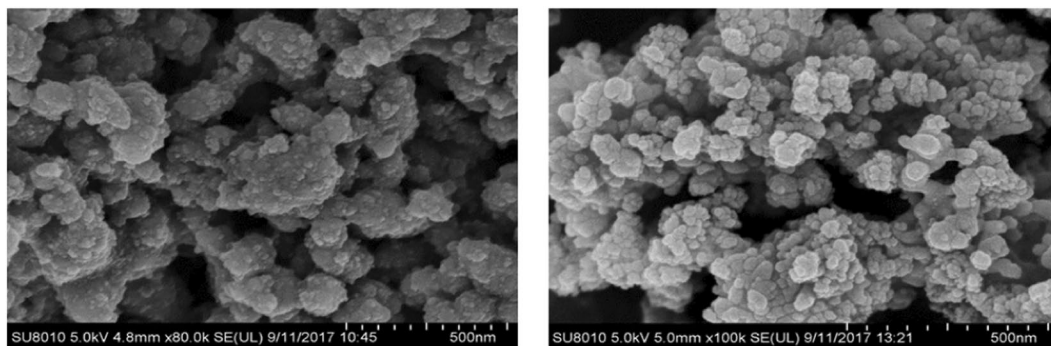


Figure 1. SEM images of meso-Fe/Co.

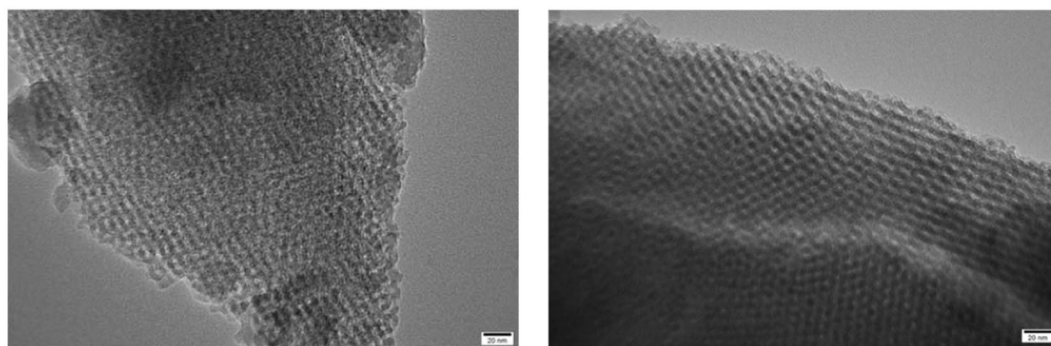


Figure 2. TEM images of meso-Fe/Co.

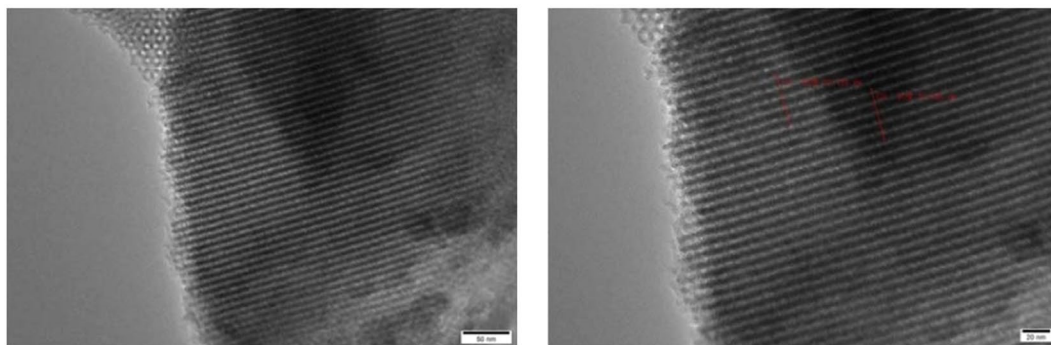


Figure 3. TEM images of KIT-6.

Studies have shown that heterogeneous catalysts with rich pore diameter and large specific surface area have excellent catalytic activity^{33–35}. Abundant pore diameter structure is not only conducive to increasing the specific surface area of the catalyst and the catalytic activity point of the catalyst, but also reducing the transfer resistance of pollutants in the pore diameter. At the same time, the catalyst has a good adsorption performance to promote the heterogeneous Fenton reaction process. The specific surface area of Mes-Fe/Co was $135.8\text{ m}^2\text{ g}^{-1}$, and the pore diameter was mainly distributed in the range of 1–40 nm. About 40% of the pore diameter was distributed in the range of 2–10 nm mesoporous, and about 20% was in the range of 10–20 nm. It is stated that the catalyst has not only a rich pore diameter structure, but also a large specific surface area indicates that the catalyst should have excellent catalytic performance.

The performance of catalysts. *Catalytic activity analysis.* UV spectrophotometric analysis of the sample helps to understand the intensity and length of time produced by $\bullet\text{OH}$, a large amount of TC was degraded and transformed, which indirectly indicated that the catalyst could catalyze the production of $\bullet\text{OH}$ for a long time. However, its production is not enough to completely degrade and mineralize the degraded and transformed TC. A large amount of TC was mineralized, indicating that the catalyst produced enough $\bullet\text{OH}$ in a certain period of

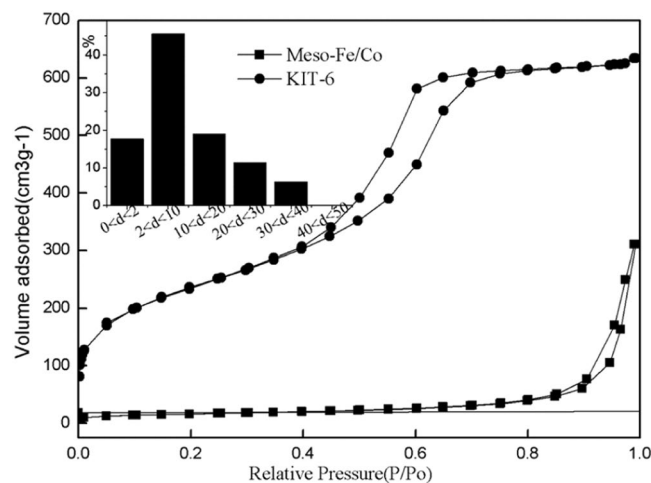


Figure 4. N_2 adsorption–desorption isotherms and pore size distribution (inset) of meso-Fe/Co.

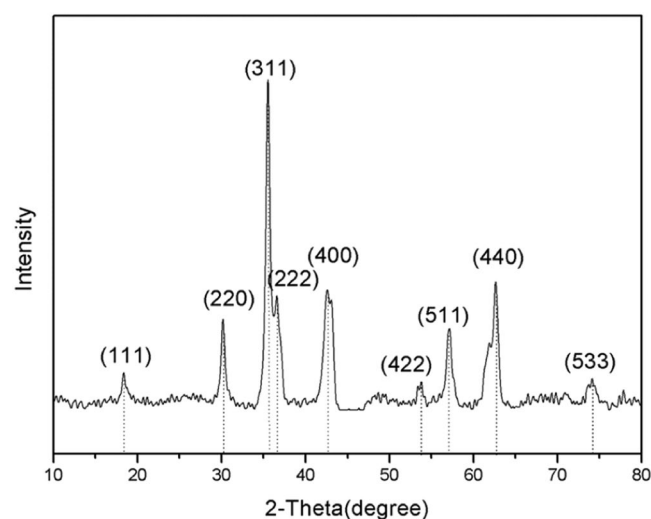


Figure 5. Wide-angle XRD patterns of meso-Fe/Co.

time. Not only can TC be degraded, but also the degradation products can be further degraded and finally mineralized effectively

The experiment was carried out with catalysts under the following conditions: Mes-Fe/Co = 0.6 g/L, H_2O_2 = 30 mmol, TC = 30 mg/L, pH = 7, $T = 25.5^\circ C$ (Fig. 6). Under the same experimental conditions, mes-Fe/Co has the best catalytic activity, which is better than any single element. Its catalytic activity is 2.7 times that of iron ion and 3.6 times that of mesoporous iron. The mineralization rate of TC in 90 minutes was over 50%, the TC degradation rate in 1.8 hours was 70%, and the TC degradation rate in 3 hours was 86%, which was similar to the result 36 reported previously^{36,37}.

Effect of iron-to-cobalt ratio. The results show that the synergistic effect of two or more metals can improve the activity of the catalyst. In order to better understand the role of cobalt in bimetallic catalysts, a series of comparative experiments were conducted (Fig. 7). The results showed that the Fenton activity at the catalyst site not only increased significantly with the increase of cobalt content, but also the reaction speed of Fenton. However, when the content of cobalt increased to a certain value, the activity of the catalyst decreased. The best Fenton properties were found in catalysts with Fe/Co molar ratios of 2:1 and 1:1. This shows that the co-action between iron and cobalt is more favorable near the 1:1 ratio of iron and cobalt.

Effect of pH. Since most discharges have an acidic or alkaline pH, the optimal pH for most chemical, physical, and biological reactions is near neutral. The pH values before and after the reaction are often adjusted to ensure pollutant removal and wastewater discharge requirements. Therefore, the study on highly active Fenton-like catalyst in different pH (Fig. 8) has an obvious usage prospective and economic value. The results reveal that the removal efficiency of catalyst at pH = 5–9 was better than that of catalyst at pH = 3 and 11. The removal

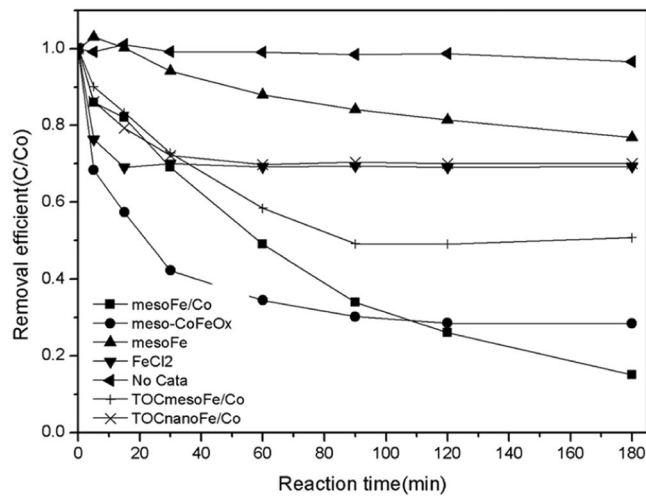


Figure 6. Performance comparison of different catalysts.

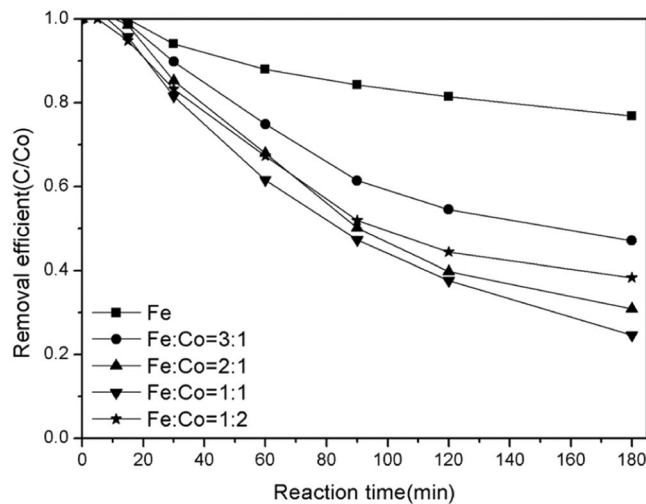


Figure 7. Effect of Fe/Co ratios on catalyst performance.

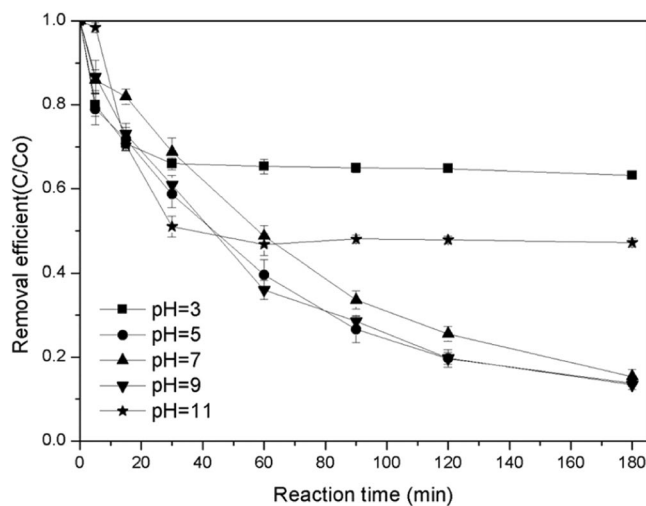


Figure 8. Effect of pH on catalyst performance.

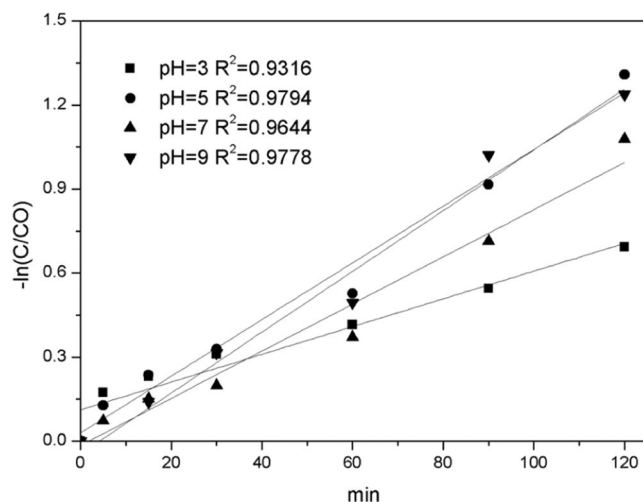


Figure 9. Pseudo first-order dynamic analysis of TC removal under different pH conditions.

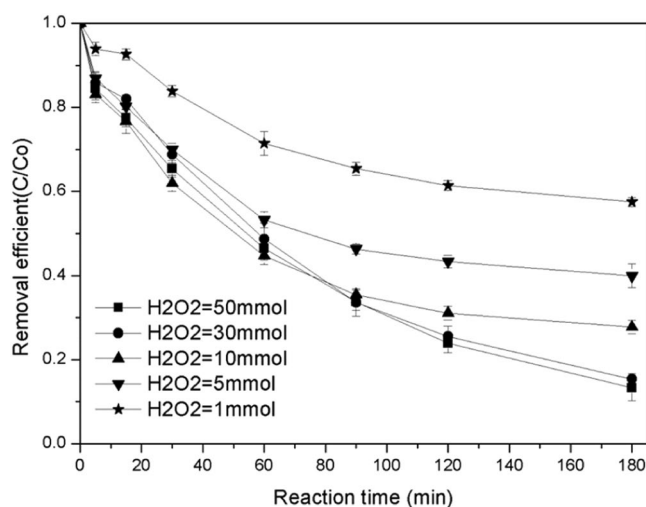


Figure 10. Effect of H_2O_2 concentration on catalyst performance.

rate of TC at pH 5–9 can reach 90%, indicating that bimetallic Fe/Co can degrade TC in a larger pH range. Pseudo-first-order reaction kinetics can better explain this process (Fig. 9). At a pH of 5, 7 and 9, the removal rate constants (k) were 0.01, 0.084 and 0.011 min^{-1} , respectively, which were 2.1, 17.8 and 2.3 times of these at a pH of 3 (0.0047), respectively. However, removal efficiency is also relatively low at a high pH. Literature reported that H_2O_2 does not produce hydroxyl group at high a pH^{21,38}. The pseudo-first-order model can well explain the degradation kinetics curve of TC, as shown below¹¹:

$$-\ln(C/C_0) = kt + b$$

where k is the pseudo first-order rate constant, C_0 is the initial concentration, and C is the concentration at time t .

Effect of H_2O_2 concentration. Hydroxyl radicals are produced from hydrogen peroxide, which acts as the actual oxidant for the removal of TC. The amount of H_2O_2 has a direct effect on the mineralization of TC degradation. The results showed (Fig. 10) that TC degradation efficiency increased from 42.5% to 86.7% with increasing H_2O_2 concentration from 1 to 50 mmol. However, when the content of H_2O_2 exceeds 30 mmol, the degradation efficiency of TC has no obviously increases. According to the pseudo-first-order reaction kinetics, the k value of TC degradation efficiency at 30 mmol was 1.6 times higher than that at 10 mmol (Fig. 11). The results suggested that high H_2O_2 concentration can promote effective contact with the catalyst and promote the reaction of $\bullet OH$ and TC within a certain concentration range (Eq. 1, 2). However, if the concentration of H_2O_2 is too high (>30 mmol), the reaction of $\bullet OH$ with H_2O_2 and $\bullet O_2H$ may be promoted (Eq. 3, 4), leading to the scavenging effect of $\bullet OH$ ^{39–41}.

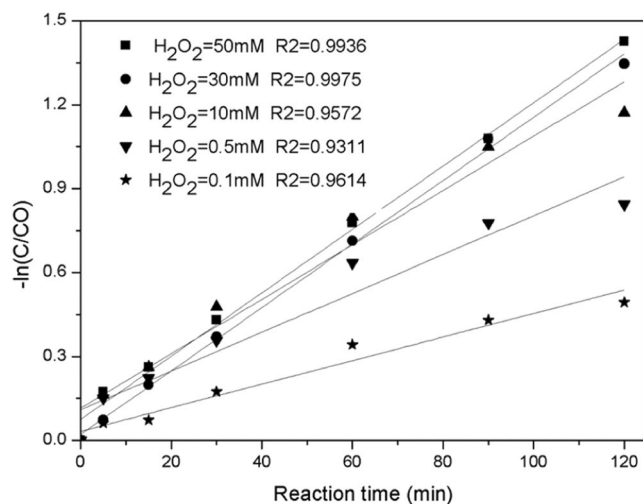


Figure 11. Pseudo first-order dynamic analysis of TC removal under different H₂O₂ conditions.

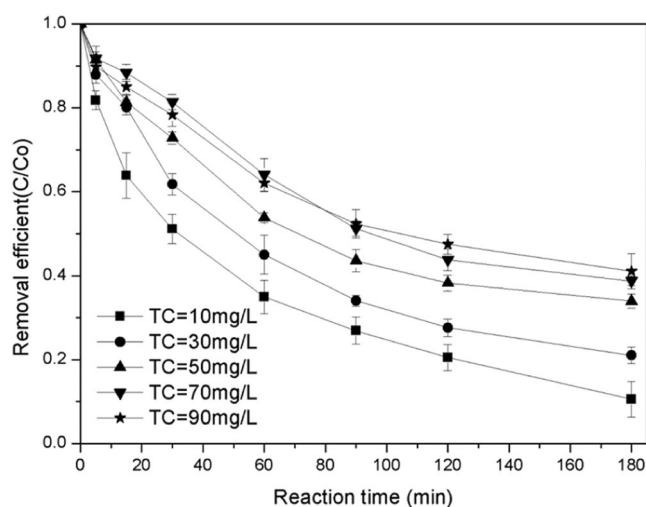


Figure 12. Effect of TC concentration on catalyst performance.



Influence of pollutant concentration on catalyst performance. The removal rate of TC gradually decreases with an increase in pollutant concentrations (Fig. 12). The removal rates of TC ranged from 89.4% to 58.92% when the concentrations of TC ranged from 10 mg/L to 90 mg/L. In the first five minutes after the reaction began, higher reaction rates were observed at all concentration levels because of the maximum values of H₂O₂ and the contaminant. The generation rate of free radical and its probability of exposure to the contaminants were at the maximum level. However, with the consumption of pollutants and H₂O₂, the production of free radicals decreased, as well as the probability of exposure to TC; thus, the degradation reaction of TC was mild. According to the first-order reaction model (Fig. 13), the reaction rate decreases with an increase in the concentration of the pollutant, but the degradation rate does not change with pollutant concentration when the pollutant concentration is higher than 50 mg·L⁻¹. This is because the catalyst surface area and the amount of H₂O₂ are the main factors limiting the production of free radicals at high concentrations. Therefore, low concentrations are conducive to the degradation

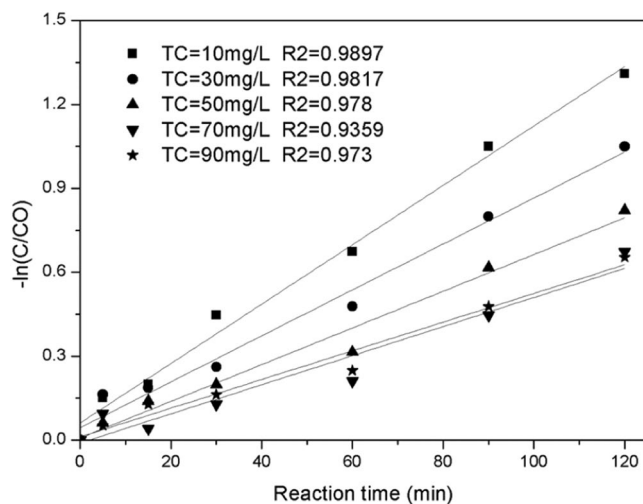


Figure 13. Pseudo first-order dynamic analysis of TC removal under different TC conditions.

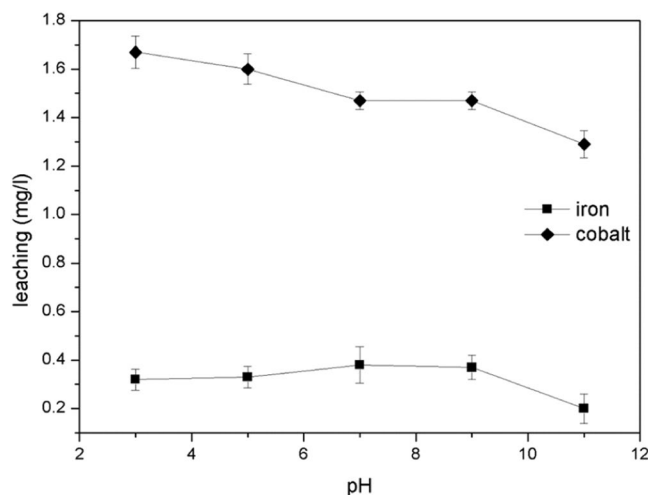


Figure 14. Concentration of iron leaching in solution during TC degradation in 3 h.

and mineralization of pollutants, whereas high concentrations are more conducive to the efficient use of H_2O_2 and the decomposition of pollutants into small molecules.

Catalytic stability of meso-Fe/Co. Successive experiments were conducted to evaluate the catalyst stability. Previous studies showed that when solution is acidic, the concentration of H^+ in the Fenton-like reaction are very high; This is not conducive to the stability of the catalyst and can accelerate the dissolution of active components iron and cobalt³⁸. After 180 min of reaction under different pH values (from 3 to 11), the precipitation of cobalt gradually decreased (1.66 mg/L, 1.6 mg/L, 1.5 mg/L, 1.5 mg/L, 1.3 mg/L) whereas the precipitation of iron was not affected by pH (0.31 mg/L, 0.33 mg/L, 0.36 mg/L, 0.37 mg/L), although it was 0.20 mg/L at pH 11 (Fig. 14). These samples had lower leaching degrees than nano- Fe_3O_4 (2.3 mg/L) and Fe_3O_4 (9.8 mg/L after 180 min) as reported previously³⁰. The leaching of Fe ions is kept below 1 mg/L, which is acceptable according to the European Union and the United States discharge standards (<2 ppm)⁴². The cobalt ion leaching also meets China's Environmental Quality Standards for Surface Water (<2 ppm) (GB 3838-2002). Thus, the treated pollutants can be discharged directly without worrying about heavy metal pollution, which is beneficial from the perspective of long-term ecological environment protection and development.

Catalytic reactions are repeated many times in succession, the activity of the catalyst decreased gradually after four successive catalytic degradation reactions (Fig. 15). Possible reasons for the decrease of catalyst activity: 1) Fe and Co ions on the surface of the catalyst form stable complexes with ^-OH in the solution, leading to the decrease of the number of active sites on the surface of the catalyst; 2) the active components Fe and Co at the active site of the catalyst were dissolved from the surface. This study revealed that catalyst deactivation has many factors, including reduced catalyst surface area, catalyst poisoning, and active ingredient dissolution. Research is needed to further explore these factors.

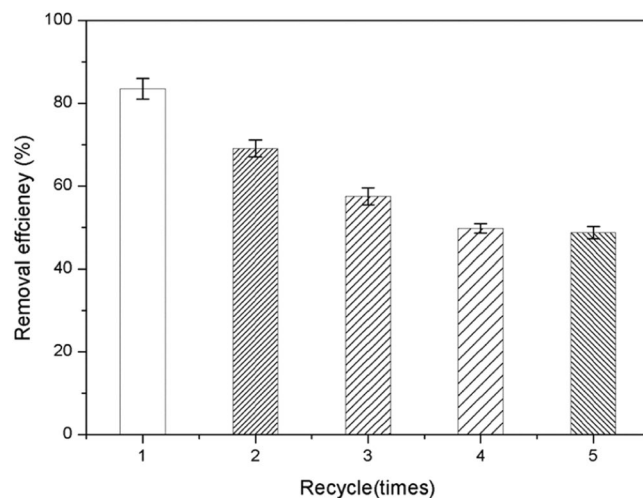


Figure 15. Catalytic activity of meso-Fe/Co composite in different cycling numbers.

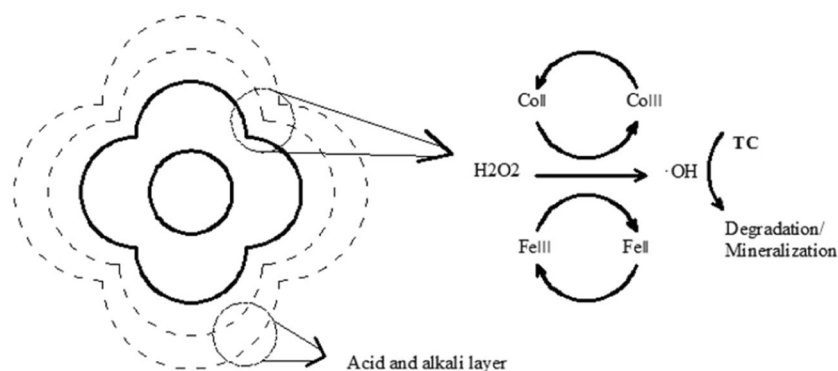
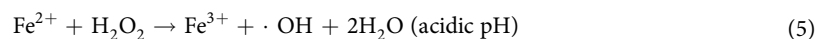


Figure 16. Schematic illustration of the reaction mechanism of H_2O_2 activation by meso-Fe/Co.

Potential mechanisms. In general, the pH required for the Fenton or Fenton-like reaction is about 3, and when the pH of the reaction solution is higher than 6, the Fenton or Fenton-like reaction is not excited. In this study, the reaction solution is still active when exceeding a pH of 9. Possible reasons for this phenomenon follow as: (1) Co has a Fenton property similar to Fe^{2+} , which can activate H_2O_2 to generate free radicals under a wide range of acid-base conditions (Eqs 5, 6)³⁹ (Fig. 16), so that the Fenton reaction can continue^{5,43–45}; (2) Co has Lewis acidity, which can form an acid-base complex as an electron pair acceptor and a hydroxide electron pair in the solution, forming an acidic or slightly acidic environment around the catalyst^{46,47}. The hydroxide stability of Co is stronger than that of iron Fe ^{48,49}. Meanwhile, the hydroxide stability can reduce the deactivation amount of Fe element and promote the Fenton or Fenton-like reaction of Fe element.



Conclusions

The Meso-Fe/Co heterogeneous Fenton catalyst was successfully prepared by template method. Qualitative and quantitative characterization of meso-Fe/Co catalyst by TEM, SEM and BET showed that meso-Fe/Co catalyst has not only a large specific surface area $113.8 \text{ m}^2\text{g}^{-1}$, but also a large number of mesoporous pore diameter distribution. Catalytic performance and operating parameters show that meso-Fe/Co catalysts have a satisfactory removal

effect on TC (86%), a good stability (precipitation cobalt and iron were less than 1.66 mg/L and 0.33 mg/L) and a wider range of pH use (good removal efficiency in 5–9 range). Therefore, the high catalytic efficiency, a smaller amount of leached ions, a wider pH application range of bimetallic Fe/Co and its convenient recycling without any regeneration made the catalyst attractive for potential applications. Unfortunately, the XPS characterization and the generation of catalyst microenvironment were not verified by corresponding experiments due to objective factors and experimental conditions.

Received: 24 August 2018; Accepted: 10 October 2019;

Published online: 01 November 2019

References

- Rizzo, L. *et al.* Urban wastewater treatment plants as hotspots for the release of antibiotics in the environment: A review. *Water Res.* **47**, 957–995 (2013).
- Zhang, Q. Q. *et al.* Comprehensive Evaluation of Antibiotics Emission and Fate in the River Basins of China: Source Analysis, Multimedia Modeling, and Linkage to Bacterial Resistance. *Environ. Sci. Technol.* **49**, 6772–6782 (2015).
- Kim, S. *et al.* Removal of Antibiotics in Wastewater: Effect of Hydraulic and Solid Retention Times on the Fate of Tetracycline in the Activated Sludge Process. *Environ. Sci. Technol.* **39**, 5816–5823 (2005).
- Munoz, M. *et al.* A ferromagnetic-alumina-supported iron catalyst for CWPO. Application to chlorophenols. *Appl. Catal. B: Environ.* **136–137**, 218–224 (2013).
- Su, S. *et al.* Heterogeneous activation of Oxone by $\text{Co}_{(x)}\text{Fe}_{(3-x)}\text{O}_4$ nanocatalysts for degradation of rhodamine B. *J Hazard Mater* **244–245**, 736–742 (2013).
- Al-Shamsi, M. A., Thomson, N. R. & Forsey, S. P. Iron based bimetallic nanoparticles to activate peroxygens. *Chem. Eng. J.* **232**, 555–563 (2013).
- Qiu, B. *et al.* Ultradispersed Cobalt Ferrite Nanoparticles Assembled in Graphene Aerogel for Continuous Photo-Fenton Reaction and Enhanced Lithium Storage Performance. *Sci. Rep.* **6**, 1–10 (2016).
- Yu, L. *et al.* Degradation of phenol using Fe_3O_4 -GO nanocomposite as a heterogeneous photo-Fenton catalyst. *Sep. Purif. Technol.* **171**, 80–87 (2016).
- Wan, Z. *et al.* Removal of sulfamethazine antibiotics using CeFe-graphene nanocomposite as catalyst by Fenton-like process. *J. Environ. Manage.* **182**, 284–291 (2016).
- Cong, Y. *et al.* Synthesis of α - $\text{Fe}_2\text{O}_3/\text{TiO}_2$ nanotube arrays for photoelectro-Fenton degradation of phenol. *Chem. Eng. J.* **191**, 356–363 (2012).
- Du, D., Wang, L. & Zhang, J. L. Yolk-shell structured $\text{Fe}_3\text{O}_4/\text{void}@\text{TiO}_2$ as a photo-Fenton-like catalyst for the extremely efficient elimination of tetracycline. *Appl. Catal. B: Environ.* **200**, 484–492 (2017).
- Wang, Y. B. *et al.* Magnetic ordered mesoporous copper ferrite as a heterogeneous Fenton catalyst for the degradation of imidacloprid. *Appl. Catal. B: Environ.* **147**, 534–545 (2014).
- Ling, Y. H. *et al.* Magnetically separable core-shell structural gamma- $\text{Fe}_2\text{O}_3/\text{Cu}/\text{Al-MCM-41}$ nanocomposite and its performance in heterogeneous Fenton catalysis. *J Hazard Mater* **264**, 195–202 (2014).
- Nguyen, T. D. *et al.* Magnetic Fe_2MO_4 (M:Fe, Mn) activated carbons: fabrication, characterization and heterogeneous Fenton oxidation of methyl orange. *J Hazard Mater* **185**, 653–661 (2011).
- Sun, B. *et al.* Prehydrolysis approach to direct synthesis of Fe, Al, Cr-incorporated SBA-15 with good hydrothermal stability and enhanced acidity. *Micropor Mesopor Mat* **186**, 14–20 (2014).
- Vickers, S. M. *et al.* Mesoporous Mn- and La-doped cerium oxide/cobalt oxide mixed metal catalysts for methane oxidation. *ACS Appl Mater Inter* **7**, 11460–11466 (2015).
- Wang, D. & Astruc, D. The recent development of efficient Earth-abundant transition-metal nanocatalysts. *Chem. Soc. Rev.* **46**, 816–854 (2017).
- Abe, H., Liu, J. & Ariga, K. Catalytic nanoarchitectonics for environmentally compatible energy generation. *Mater. Today* **19**, 12–18 (2016).
- Didehban, K. *et al.* Nanocatalysts for C–Se cross-coupling reactions. *RSC Adv.* **8**, 291–301 (2018).
- Coker, V. S. *et al.* Probing the site occupancies of Co-, Ni-, and Mn-substituted biogenic magnetite using XAS and XMCD. *Am. Mineral.* **93**, 1119–1132 (2008).
- Deng, J. H. *et al.* FeVO_4 as a highly active heterogeneous Fenton-like catalyst towards the degradation of Orange II. *Appl. Catal. B: Environ.* **84**, 468–473 (2008).
- Saptiama, I. *et al.* Mesoporous Alumina as an Effective Adsorbent for Molybdenum (Mo) toward Instant Production of Radioisotope for Medical Use. *Bull. Chem. Soc. Jpn.* **90**, 1174–1179 (2017).
- Saptiama, I. *et al.* Molybdenum Adsorption Properties of Alumina-Embedded Mesoporous Silica for Medical Radioisotope Production. *Bull. Chem. Soc. Jpn.* **91**, 195–200 (2018).
- Li, W. *et al.* Mesoporous materials for energy conversion and storage devices. *Nat Rev Mater* **1**, 1–17 (2016).
- Tang, F. Q. *et al.* Mesoporous Silica Nanoparticles: Synthesis, Biocompatibility and Drug Delivery. *Adv. Mater.* **24**, 1504–1534 (2012).
- Lv, Q. *et al.* Preparation of magnetic core/shell structured γ - $\text{Fe}_2\text{O}_3/\text{Ti-tmSiO}_2$ and its application for the adsorption and degradation of dyes. *Micropor Mesopor Mat* **186**, 7–13 (2014).
- Kleitzi, F., Hei Choi, S. & Ryoo, R. Cubic Ia3d large mesoporous silica: synthesis and replication to platinum nanowires, carbon nanorods and carbon nanotubes. *Chem. Commun.*, 21–36 (2003).
- Tüysüz, H. *et al.* Synthesis of Hard Magnetic Ordered Mesoporous $\text{Co}_3\text{O}_4/\text{CoFe}_2\text{O}_4$ Nanocomposites. *Chem. Mater.* **24**, 2493–2500 (2012).
- Tamura, H. *et al.* Spectrophotometric determination of iron(II) with 1,10-phenanthroline in the presence of large amounts of iron(III). *Talanta* **21**, 314–318 (1974).
- Xu, L. J. & Wang, J. L. Fenton-like degradation of 2,4-dichlorophenol using Fe_3O_4 magnetic nanoparticles. *Appl. Catal. B: Environ.* **123–124**, 117–126 (2012).
- Yang, H. Q. *et al.* Synthesis of 5-(5-nitro-2-pyridylazo)-2,4-diaminotoluene and its application to spectrophotometric determination of microamounts of palladium. *Talanta* **43**, 747–753 (1996).
- Feng, J. Y., Hu, X. J. & Yue, P. L. Discoloration and Mineralization of Orange II Using Different Heterogeneous Catalysts Containing Fe. A Comparative Study. *Environ. Sci. Technol.* **38**, 5773–5778 (2004).
- Yao, Y. J. *et al.* Fe, Co, Ni nanocrystals encapsulated in nitrogen-doped carbon nanotubes as Fenton-like catalysts for organic pollutant removal. *J Hazard Mater* **314**, 129–139 (2016).
- Gao, G., Sun, R. J. & Cui, D. X. Ultrafine ferroferric oxide nanoparticles embedded into mesoporous carbon nanotubes for lithium ion batteries. *Sci. Rep.* **5**, 17553 (2015).
- Li, X. F. *et al.* Highly dispersed Pd/PdO/ Fe_2O_3 nanoparticles in SBA-15 for Fenton-like processes: confinement and synergistic effects. *Appl. Catal. B: Environ.* **165**, 79–86 (2015).

36. Pouredetal, H. R. & Sadegh, N. Effective removal of Amoxicillin, Cephalexin, Tetracycline and Penicillin G from aqueous solutions using activated carbon nanoparticles prepared from vine wood. *Journal of Water Process Engineering* **1**, 64–73 (2014).
37. Zhu, X. D. *et al.* Photocatalytic degradation of tetracycline in aqueous solution by nanosized TiO₂. *Chemosphere* **92**, 925–932 (2013).
38. Zhou, C. S. *et al.* Fe₃-xCu_xO₄ as highly active heterogeneous Fenton-like catalysts toward elemental mercury removal. *Chemosphere* **125**, 16–24 (2015).
39. Albuquerque, A. S. *et al.* Nanostructured ferrites: Structural analysis and catalytic activity. *Ceram. Int.* **38**, 2225–2231 (2012).
40. Wei, L. *et al.* Efficient Removal of Organic Pollutants with Magnetic Nanoscaled BiFeO₃ as a Reusable Heterogeneous Fenton-Like Catalyst. *Environ. Sci. Technol.* **44**, 1786–1791 (2010).
41. Xu, L. J. & Wang, J. L. A heterogeneous Fenton-like system with nanoparticulate zero-valent iron for removal of 4-chloro-3-methyl phenol. *J Hazard Mater* **186**, 256–264 (2011).
42. Yang, X. J. *et al.* Iron oxychloride (FeOCl): an efficient Fenton-like catalyst for producing hydroxyl radicals in degradation of organic contaminants. *J. Am. Chem. Soc.* **135**, 16058 (2013).
43. Ross, P. N. R. E. H. A. B. Rate Constants for Reactions of Inorganic Radicals in Aqueous Solution. *Journal Physical and Chemical Reference Data* **17**, 1027–1284 (1988).
44. Fernandez, J. *et al.* Bleaching and photobleaching of Orange II within seconds by the oxone/Co²⁺ reagent in Fenton-like processes. *Appl. Catal. B: Environ.* **49**, 207–215 (2004).
45. Wang, Y. R. & Chu, W. Degradation of a xanthene dye by Fe(II)-mediated activation of Oxone process. *J Hazard Mater* **186**, 1455–1461 (2011).
46. Anipsitakis, G. P. & Dionysiou, D. D. D. Radical generation by the interaction of transition metals with common oxidants. *Environ. Sci. Technol.* **38**, 3705–3712 (2004).
47. Xia, M. *et al.* Magnetically separable mesoporous silica nanocomposite and its application in Fenton catalysis. *Micropor Mesopor Mat* **145**, 217–223 (2011).
48. Li, S. S. & Gurol, M. D. Catalytic decomposition of hydrogen peroxide on iron oxide_ kinetics, mechanism, and implications. *Environ. Sci. Technol.* **32**, 1417–1423 (1988).
49. Yang, Q. J. *et al.* Iron–cobalt mixed oxide nanocatalysts: Heterogeneous peroxymonosulfate activation, cobalt leaching, and ferromagnetic properties for environmental applications. *Appl. Catal. B: Environ.* **88**, 462–469 (2009).

Acknowledgements

The authors would like to thank the National Key R&D Program of China (2018YFD1100505) and Guangxi Innovation Drives Development Special Fund Project (No. AA17202032-3) and Major Science and Technology Program for Water Pollution Control and Treatment (No. 2014ZX07504003) for the financial support.

Author contributions

This manuscript was designed and implemented by Dr. Jinyuan Jiang and Junchao Li. Dr. Xuhua Li and Dr. Fansheng Meng guided and assisted the whole experiment process and manuscript. Jindong Han participated in the implementation of the experiment and data analysis and provided considerable help. Dr. Jiao Li and Dr. Chunlian Xu, Yun Li provided the necessary funding for the manuscript and the trial. Here, I would like to thank all the doctors and students for their efforts and dedication to this manuscript.

Competing interests

The authors declare no competing interests.

Additional information

Correspondence and requests for materials should be addressed to J.J.

Reprints and permissions information is available at www.nature.com/reprints.

Publisher's note Springer Nature remains neutral with regard to jurisdictional claims in published maps and institutional affiliations.



Open Access This article is licensed under a Creative Commons Attribution 4.0 International License, which permits use, sharing, adaptation, distribution and reproduction in any medium or format, as long as you give appropriate credit to the original author(s) and the source, provide a link to the Creative Commons license, and indicate if changes were made. The images or other third party material in this article are included in the article's Creative Commons license, unless indicated otherwise in a credit line to the material. If material is not included in the article's Creative Commons license and your intended use is not permitted by statutory regulation or exceeds the permitted use, you will need to obtain permission directly from the copyright holder. To view a copy of this license, visit <http://creativecommons.org/licenses/by/4.0/>.

© The Author(s) 2019